Applied Physics Letters ARTICLE scitation.org/journal/apl

# Molecular beam homoepitaxy on bulk AlN enabled by aluminum-assisted surface cleaning

Cite as: Appl. Phys. Lett. **116**, 172106 (2020); doi: 10.1063/1.5143968
Submitted: 27 December 2019 · Accepted: 11 April 2020 ·
Published Online: 29 April 2020



YongJin Cho,[1,a] Celesta S. Chang,[2,3] Kevin Lee,[1] Mingli Gong,[4] Kazuki Nomoto,[1] Masato Toita,[5] Leo J. Schowalter,[5] David A. Muller,[3,6] Debdeep Jena,[1,4,6] and Huili Grace Xing[1,4,6]

## AFFILIATIONS

[1]School of Electrical and Computer Engineering, Cornell University, Ithaca, New York 14853, USA
[2]Department of Physics, Cornell University, Ithaca, New York 14853, USA
[3]School of Applied and Engineering Physics, Cornell University, Ithaca, New York 14853, USA
[4]Department of Materials Science and Engineering, Cornell University, Ithaca, New York 14853, USA
[5]Crystal IS, Green Island, New York 12183, USA
[6]Kavli Institute for Nanoscale Science, Cornell University, Ithaca, New York 14853, USA

[a]**Author to whom correspondence should be addressed:** yongjin.cho@cornell.edu

## ABSTRACT

We compare the effectiveness of *in situ* thermal cleaning with that of Al-assisted cleaning of native surface oxides of bulk AlN for homoepitaxial growth by molecular beam epitaxy. Thermal deoxidation performed at 1450 °C in vacuum results in voids in the AlN substrate. On the other hand, Al-assisted deoxidation at ≈900°C results in high-quality AlN homoepitaxy, evidenced by clean and wide atomic terraces on the surface and no extended defects at the growth interface. This study shows that Al-assisted *in situ* deoxidation is effective in removing native oxides on AlN, providing a clean surface to enable homoepitaxial growth of AlN and its heterostructures; furthermore, it is more attractive over thermal deoxidation, which needs to be conducted at much higher temperatures due to the strong bonding strength of native oxides on AlN.



AlN is an ultrawide-bandgap semiconductor with a high thermal conductivity and high piezoelectricity. The combination of a wide bandgap of $E_g \approx 6.1$ eV, high piezoelectricity, and a large thermal conductivity of $\kappa \approx 340$ W/m · K makes AlN a critical material for advancing applications in micro electro-mechanical systems (MEMS), ultraviolet photonics, and high power electronics that can sustain high temperatures and harsh environments.[1–7] For MEMS and electronic and photonic devices, AlN is typically grown heteroepitaxially on substrates such as silicon, sapphire, and SiC.[8] In the past two decades, the technology of bulk AlN growth has advanced significantly; high-quality single-crystal AlN substrates with a low dislocation density are now commercially available. Deep ultra-violet (DUV) light emitting diodes (LEDs) on AlN substrates with emission wavelengths as short as 200 nm are now available.[9] Very recently, Zhang *et al.* reported the shortest wavelength room temperature electrically injected DUV laser diodes emitting at 271.8 nm.[10] This remarkable achievement was enabled by AlN bulk substrates with a very low density of dislocations ($\approx 10^4$ cm$^{-2}$) and utilizing low-loss cladding layers using polarization-induced *p*-type doping.[11] These DUV laser diode heterostructures were grown by metal-organic chemical vapor deposition. However, little work on AlN homoepitaxy by molecular beam epitaxy (MBE) has been reported. A major hurdle in achieving true homoepitaxial growth of AlN by MBE is the difficulty in removing native surface oxides. This surface layer has been identified to be a mixture of AlOOH,[12] Al(OH$_3$),[12] and $\theta$-Al$_2$O$_3$.[13] Such Al$_x$O$_y$N$_z$-based materials possess high bond energies, making their *in situ* removal problematic. If the surface oxide is successfully removed *ex situ*, the AlN surface oxidizes rapidly in ambient conditions, making it difficult to start with an oxide-free AlN surface for MBE growth. With the rapid improvement in the quality and availability of AlN bulk substrates, it is timely to develop *in situ* methods to deoxidize the AlN surface and enable clean homoepitaxial growth by MBE.

It is known that surface oxygen atoms on *c*-plane $\alpha$-Al$_2$O$_3$ start desorbing above 1300 °C in vacuum, leading to an Al-rich $(\sqrt{31} \times \sqrt{31})R \pm 9°$ surface reconstruction.[14–16] To attempt *in situ* thermal cleaning of native surface oxides of AlN at such temperatures, an ultra-high-temperature MBE system is required,[16,17] which is used for the experiments reported in this work. Meanwhile, metal-assisted deoxidation using Ga[18,19] and In[20,21] has been widely used for the MBE growth of many technologically important compound semiconductors including GaAs and GaN. Al-assisted deoxidation of Al$_2$O$_3$ has also been reported for forming volatile Al$_2$O following the reaction $Al_2O_3 + 4Al \rightarrow 3Al_2O\nearrow$.[22,23] In this work, by

performing a comparative study of two *in situ* deoxidation methods for AlN homoepitaxy by MBE, it is found that dramatically improved AlN homoepitaxy can be enabled by Al-assisted *in situ* deoxidation at moderate temperatures achievable in most epitaxial systems.

High-structural-quality Al-polar AlN(0001) bulk substrates[24] with a dislocation density of $\approx 10^4\,cm^{-2}$ produced by Crystal IS were used as the substrates in this study. The MBE growth of AlN epilayers was performed in an ultra-high-temperature Veeco GENxplor chamber equipped with a standard effusion cell for Al and a radio frequency plasma source for active N species. The base pressures of the growth chamber were $\approx 10^{-10}$ Torr under idle conditions and $\approx 2 \times 10^{-5}$ Torr during growth due to $N_2$. The substrate surface temperature of the system was calibrated using the temperature dependent desorption flux of Al metal.[8] All temperatures in this work refer to the substrate surface temperature unless otherwise noted. After chemical cleaning in solvents and acids, followed by a final rinse with de-ionized water, the AlN substrates with an area of 1 cm × 1 cm were loaded into the MBE system and outgassed at 200 °C for 8 h. To clean the surface oxides, the first set of AlN substrates was held at 1450 °C (which is lower than the decomposition temperature[25] of 1927 °C of AlN) in the growth chamber for 2 h while keeping all MBE sources closed. The second set of AlN substrates was cleaned using multiple cycles of Al-assisted adsorption/desorption at 870 °C as described below. In order to see the impacts of the *in situ* cleaning methods, a control sample, namely, without intentional *in situ* cleaning, was also grown. Other than this difference in the *in situ* deoxidation methods, the subsequent homoepitaxial growth was performed on the three sets under nominally identical conditions. 200 − 300 nm thick AlN layers were grown at 910 °C under Al-rich conditions ($\phi_{Al} = 12\,nm\,min^{-1}$) at a growth rate of $5\,nm\,min^{-1}$ ($=\phi_N$), where $\phi_{Al}$ and $\phi_N$ are the Al and N fluxes, respectively. A more detailed account describing the growth conditions for AlN homoepitaxy by MBE will be presented elsewhere.

Surface changes during the *in situ* cleaning of the AlN substrate and during and after epitaxial growth were monitored by reflection high energy electron diffraction (RHEED). Excess Al droplets after growth were thermally desorbed at the growth temperature with closed Al and N shutters; this process was monitored by the recovery of the RHEED intensity. Surface morphology was evaluated by atomic force microscopy (AFM), and structural quality was studied by scanning transmission electron microscopy (STEM) and x-ray diffraction (XRD). XRD measurements were performed with a high-resolution x-ray source (Cu $K\alpha_1$: $\lambda = 0.154056$ nm) of a PANalytical X'Pert Pro system equipped with a Ge(220) monochromator. Cross-sectional TEM samples of AlN were prepared using a Helios G4 UX focused ion beam (FIB) with the finishing voltage of 5 keV. Samples were coated with carbon and platinum prior to milling to reduce surface damage. The samples were then compared by images acquired by STEM using an aberration corrected Titan Themis operating at 300 keV. The impact of the *in situ* cleaning method on the densities of O, Si, H, and C impurities in epilayer/substrate interface regions was studied by secondary ion mass spectrometry (SIMS).

We first study how the AlN substrate surface evolves during *in situ* cleaning. The AlN bulk substrate without any *in situ* cleaning shows smooth surface morphology, as evidenced by streaky RHEED patterns [Fig. 1(a)]. The spotty RHEED patterns [Fig. 1(b)] of the thermally cleaned sample imply that the surface becomes rough after thermal cleaning. Such roughening by thermal deoxidation is

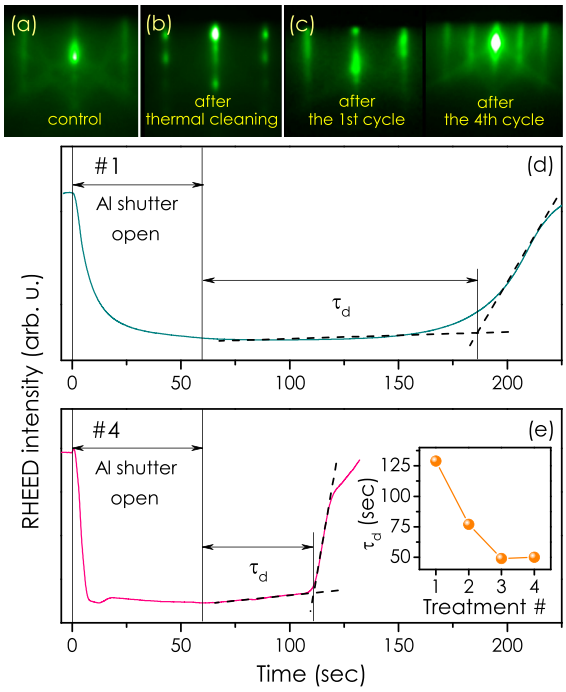


**FIG. 1.** RHEED patterns of the AlN substrate (a) without any *in situ* cleaning, (b) after thermal cleaning at 1450 °C, and (c) after Al-assisted cleaning. All the RHEED patterns were taken along the $\langle 11\bar{2}0 \rangle$ azimuth. [(d) and (e)] Variation of the specular RHEED intensity in vacuum (i.e., $\phi_N = 0$) upon adsorption of Al ($\phi_{Al} = 4$ nm $min^{-1}$) for 60 s and subsequent desorption at a substrate temperature of 870° C for the first treatment (d) and the fourth treatment (e), and (c) the corresponding RHEED patterns taken after the respective Al desorption. The Al shutter was opened only during the Al deposition and was closed for other times. Note the spotty patterns in (b), indicating the rough surface, and the (2 × 2) surface reconstruction in (c), indicating the metal-poor metal-polar III-N surface.

commonly observed for GaAs,[26] where the corresponding deoxidation process accompanies the consumption of GaAs via $4GaAs + Ga_2O_3 \rightarrow Ga_2O\nearrow + 2As_2\nearrow$.[27] A similar process is believed to occur for the thermal deoxidation of AlN, namely, $4AlN + Al_2O_3 \rightarrow Al_2O\nearrow + 2N_2\nearrow$. Figures 1(d) and 1(e) show the evolution of the specular RHEED intensity observed during the Al-assisted cleaning process of Al metal adsorption and desorption at a substrate temperature of 870 °C. Here, the Al flux is $\phi_{Al} = 4\,nm\,min^{-1}$, and the Al shutter is opened for 60 s for each cycle. During this Al-assisted cleaning process, the N source was under idle conditions: zero plasma power and zero $N_2$ gas flow rate. It is essential that this Al-assisted cleaning is performed without active N species in order to avoid any unintentional AlN formation by any active N during cleaning. Even though the same Al flux and deposition time were applied in each cycle, the time evolution of the RHEED intensity is seen to change significantly with a repeated Al-assisted cleaning cycle. For the first cycle, the RHEED intensity is seen to gradually change with time. As the number of Al-treatments increases, the evolution of the RHEED intensity starts, resembling what is typically observed during Ga adsorption/desorption on clean GaN surfaces.[28–30] For GaN surfaces, upon Ga adsorption, the RHEED intensity first quenches rapidly due to Ga adlayer formation, and after this initial rapid drop, it decreases at a slower rate due to the

accumulation of Ga droplets. Once the metal shutter is closed, the RHEED intensity increases at a slow rate due to the desorption of Ga droplets and finally recovers rapidly due to Ga adlayer desorption.

Guided by the well understood Ga adsorption/desorption kinetics on the GaN surface,[28–30] the delay observed in the RHEED intensity recovery after the Al shutter is closed can be understood as the time for Al droplet desorption. In order to quantify it, we define a desorption time $\tau_d$ of Al droplets as the time interval between the closing of the Al shutter and a point of contact time between two linear slopes, corresponding to the respective droplet and adlayer desorption, as shown in Figs. 1(d) and 1(e). This definition of $\tau_d$ is chosen for convenience: desorption also occurs during adsorption. As the Al-assisted treatment number $n$ increases, $\tau_d$ decreases monotonically and saturates for $n > 3$. Figure 1(c) shows RHEED images taken after the first and fourth cleaning cycles, i.e., after the full recovery of the RHEED intensity. Once the intensity is fully recovered (saturated), the RHEED patterns were seen not to depend on when it is taken. It is also important to note that for $n > 3$, the surface starts to show $(2 \times 2)$ surface reconstruction [Fig. 1(c)], which is typically observed for metal-poor, metal-polar nitride surfaces.[31–33] The dependence of $\tau_d$ on the treatment number, for the fixed $\phi_{Al}$ and substrate temperature, implies that Al adatoms have different lifetimes on the respective surface. Two surface reactions are expected: (1) oxide removal via $4Al + Al_2O_3 \rightarrow 3Al_2O\nearrow$ and (2) Al droplet formation and desorption. Because the Al−Al bond in Al droplets has a low activation energy for desorption, the corresponding desorption process (and the concomitant recovery of RHEED intensity) is expected to be fast. Thus, from the observed saturation of $\tau_d$ with $n$, it can be inferred that the surface oxide has been gradually removed by Al-assisted cleaning.

We now discuss the effects of the two *in situ* cleaning methods on AlN homoepitaxy. First, the control sample, without *in situ* cleaning, shows surface morphology characterized by spiral hillocks, implying the formation of dislocations [Figs. 2(a) and 2(d)]. The sample grown on the thermally cleaned AlN substrate reveals two distinct regions: smooth areas with clear atomic steps and rough regions characterized by surface pits [Figs. 2(b) and 2(e)]. Based on the size and shape of the smooth region, it is likely that Al droplets seem to enhance the mobility of adatoms, resulting in the smooth morphology. On the other hand, AlN grown on the AlN substrate, which was cleaned by Al-assisted desorption multiple times ($n = 7$), shows a very smooth surface with clear atomic steps in a wide range [Fig. 2(c)]. The height of each step of this smooth surface is very close to the one monolayer thickness of *c*-plane AlN, indicating no step-bunching [the inset of Fig. 2(f)].

The structural properties of the overgrown AlN samples were then studied using high angle annular dark field-scanning transmission electron microscopy (HAADF-STEM) and XRD. The AlN layer grown on bulk AlN without *in situ* cleaning shown in Fig. 3(a) reveals a considerable image contrast in the film due to strain from the extended defects originating from the interface. Figure 3(b) confirms AlN homoepitaxy from the same crystal structures of the substrate and the MBE-grown AlN epilayer, while the contrast implies that the growth surface was not chemically clean. On the other hand, AlN grown on the thermally cleaned AlN substrate does not have any extended defects in the MBE-grown layer [Fig. 3(d)]; there are no observable features in the interface region. However, it is seen that the bulk AlN substrate near the interface contains hollow defects. The high resolution image reveals a clear strain field developed at these voids. As the epitaxial growth temperatures were similar among the samples, the formation of such defects must be due to high-temperature cleaning. Presumably, the high temperature leads to the clustering of vacancy defects, producing local stress fields.[34,35]

In sharp contrast, the AlN epilayer grown on AlN cleaned by the Al-assisted deoxidation method does not show any strain within the layer [Fig. 3(g)], indicating greatly improved AlN homoepitaxy. The contrast within AlN in Fig. 3(g) is likely due to ion milling during

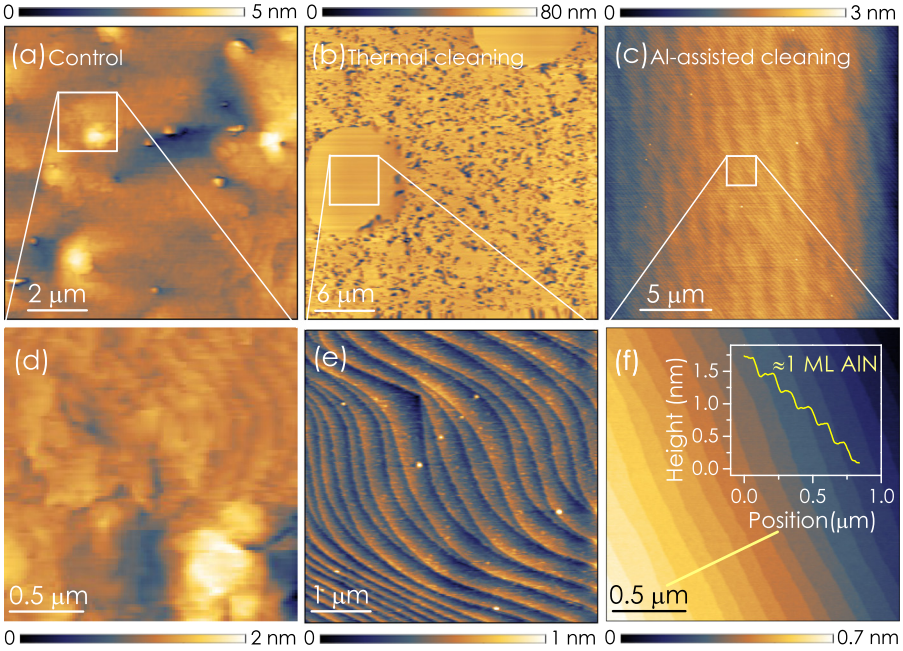


**FIG. 2.** AFM micrographs of AlN grown on AlN bulk substrates, the surface of which was not *in situ* cleaned [(a) and (d)], was thermally cleaned [(b) and (e)], and was Al-assisted cleaned [(c) and (f)]. The root mean square roughness values (scan area) of the images are (a) 0.47 nm ($10 \times 10$ $\mu m^2$), (b) 7.19 nm ($30 \times 30$ $\mu m^2$), (c) 0.34 nm ($20 \times 20$ $\mu m^2$), (d) 0.20 nm ($2 \times 2$ $\mu m^2$), (e) 0.11 nm ($5 \times 5$ $\mu m^2$), and (f) 0.10 nm ($2 \times 2$ $\mu m^2$). The inset in (f) shows the surface line profile of the yellow line in (f). Note that the step heights are close to the 1 monolayer thickness of *c*-plane AlN.

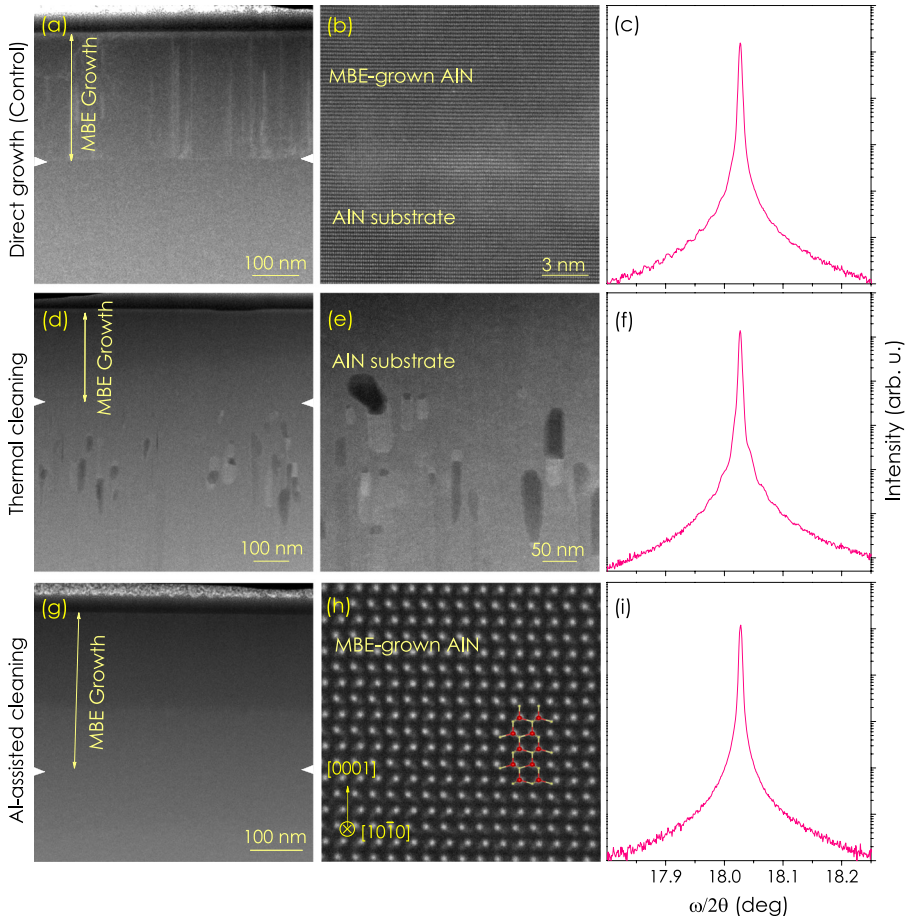


**FIG. 3.** [(a), (d), and (g)] Low magnification HAADF-STEM images, [(b), (e), and (h)] enlarged images, and [(c), (f), and (i)] symmetric XRD $\omega/2\theta$ scans of AlN grown on AlN bulk substrates, the surface of which was not *in situ* cleaned [(a), (b), and (c)], was thermally cleaned [(d), (e), and (f)], and was Al-assisted cleaned [(g), (h), and (i)]. The notches in (a), (d), and (g) indicate the growth interface. A ball-and-stick model for Al-polar AlN is superimposed on (h), where the red balls indicate the Al atoms and the tiny gray balls are the N atoms. Note the absence of thickness fringes for the sample with Al-assisted cleaning.

sample preparation [see Fig. S4 in the supplementary material]. The atomic resolution image of the MBE-grown AlN epilayer in Fig. 3(h) shows a very well-ordered Al-polar AlN crystal structure (see the overlaid crystal structure schematic) in the epilayer, with no visible defects at the growth interface [Fig. 3(g)].

A symmetric XRD $\omega/2\theta$ scan is a very sensitive tool to check the film/substrate continuity for homoepitaxy. Thickness fringes in such XRD spectra can indicate the presence of any unintentional material and/or disordered nucleation layer between the substrate and the epilayer, which is a material discontinuity along the growth direction.[36] Figures 3(c), 3(f), and 3(i) show symmetric XRD $\omega/2\theta$ scans for the three samples along the AlN (0002) Bragg reflection. The AlN epilayer grown on the AlN substrate without *in situ* cleaning clearly shows a chemically distinct interface from the thickness fringes in Fig. 3(c), with the frequency of the oscillations indicating a thickness of ≈250 nm, which is confirmed by the cross-sectional TEM image [Fig. 3(a)] and SIMS [Fig. S1 in the supplementary material]. However, the AlN sample grown upon thermal cleaning does not show fringes, but shows weak features. AlN grown on Al-assisted cleaning shows neither fringes nor any features, indicating the structural continuity of the MBE layer and the bulk substrate.

The effective deoxidation of the AlN substrate surface by Al-assisted cleaning is further confirmed by SIMS characterization. Indeed, an AlN sample grown on the AlN bulk substrate by Al-assisted cleaning shows a significantly lower (≈$10^3$ times) O concentration in the epilayer/bulk substrate interface region compared to the one grown on the AlN bulk substrate without *in situ* cleaning [see Fig. 4(a)]. AlN grown by the thermal cleaning method reveals a lower O concentration (≈$5 \times 10^{19}$ cm$^{-3}$) than the control sample but higher than the Al-assisted sample [Fig. 4(a)]. The relatively broad peak and apparently high O concentration in the substrate are presumably due to signal tailing resulting from the relatively uneven surface height [see Figs. 2(b) and S2 in the supplementary material]. Al-assisted cleaning is also effective in removing Si and H [Figs. 4(b) and 4(c)]. Judging from almost the same C concentration of the control and Al-assisted samples [Fig. 4(d)], these C impurities are currently attributed to air exposure before the bulk substrate loading, and the Al-assisted cleaning does not result in any appreciable change in C incorporation at the substrate surface. It is interesting to note that the high temperature thermal cleaning is very effective in removing Si, H, and C impurities. Specifically, almost all C impurities were removed by such a high temperature cleaning step. Nonetheless, the Al-assisted cleaning method results in peak densities of residual O and C impurities $<5 \times 10^{18}$ cm$^{-3}$ at the growth interface. Such a doping level impurity density is generally observed at many other epilayer/substrate interfaces grown by conventional epitaxy techniques.

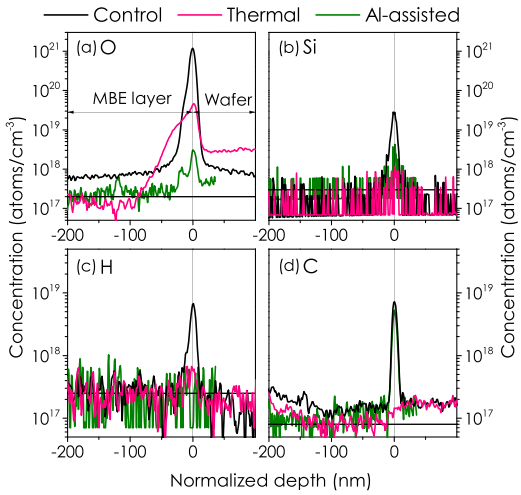


**FIG. 4.** SIMS depth profiles of (a) O, (b) Si, (c) H, and (d) C in AlN grown on the AlN bulk substrate, where the surface was not *in situ* cleaned (black lines), was thermally cleaned (pink lines), and Al-assisted cleaned (green lines). For better comparison, the spectra were horizontally shifted to match the interface regions (zero depth). The horizontal lines designate the detection limits of the corresponding elements. Note the differences in the O concentration among the samples at the interface.

The Al-assisted cleaning method results in significantly reduced O contamination on the AlN surface, enabling greatly improved AlN homoepitaxy. For a lower thermal budget, one may consider to use Ga instead of Al for deoxidation of AlN. Indeed, there have been attempts for it, but there has been no report that Ga-assisted deoxidation works for the AlN substrate. The reason is believed to be the strong bonding energy between Al and O; as a result, it is difficult for Ga to dissociate Al–O. In fact, the standard Gibbs free energy difference for the reaction $Al_2O_3+4Ga \rightarrow Al_2O\nearrow+2Ga_2O\nearrow$ is + 2.18 eV/f.u.,[37] where f.u. is formula unit, meaning that the reaction is not thermodynamically favorable. For comparison, the standard Gibbs free energy change for the reaction $Al_2O_3 + 4Al \rightarrow 3Al_2O\nearrow$ is –0.92 eV/f.u.,[37] indicating that this reaction is thermodynamically favorable, making solid $Al_2O_3$ volatile by Al metal possible.

To conclude, Al-assisted cleaning is found to be a practical and effective method to deoxidize AlN bulk substrate surfaces for achieving true homoepitaxial growth by MBE. In applying this method to AlN bulk substrates or AlN template substrates for deoxidation, one needs to remember that the deoxidation process of $Al_2O_3$ is relatively slow. This fact indicates that multiple Al-assisted cleaning cycles are required for the thorough deoxidation of the native AlN oxide.

See the supplementary material for the SIMS raw data and low magnification TEM micrograph of the Al-assisted sample.

The authors at Cornell University acknowledge partial funding support from Crystal IS, No. AFOSR FA9550-17-1-0048, and the NSF MRSEC program (No. DMR-1719875). This work made use of the shared facilities that are supported through the NSF MRSEC program (No. DMR-1719875), the MRI program (Nos. DMR-1429155 and DMR-1338010), and the NSF PARADIM program (No. DMR-1539918).

## REFERENCES

[1]Y. Taniyasu, M. Kasu, and T. Makimoto, Nature **441**, 325 (2006).
[2]H. Okumura, S. Suihkonen, J. Lemettinen, A. Uedono, Y. Zhang, D. Piedra, and T. Palacios, Jpn. J. Appl. Phys., Part 1 **57**, 04FR11 (2018).
[3]Z. Ren, Q. Sun, S.-Y. Kwon, J. Han, K. Davitt, Y. Song, A. Nurmikko, H.-K. Cho, W. Liu, J. Smart *et al.*, Appl. Phys. Lett. **91**, 051116 (2007).
[4]Z. Ren, Q. Sun, S.-Y. Kwon, J. Han, K. Davitt, Y. Song, A. Nurmikko, W. Liu, J. Smart, and L. Schowalter, Phys. Status Solidi C **4**, 2482 (2007).
[5]R. Collazo, S. Mita, J. Xie, A. Rice, J. Tweedie, R. Dalmau, and Z. Sitar, Phys. Status Solidi C **8**, 2031 (2011).
[6]M. Qi, G. Li, S. Ganguly, P. Zhao, X. Yan, J. Verma, B. Song, M. Zhu, K. Nomoto, H. Xing *et al.*, Appl. Phys. Lett. **110**, 063501 (2017).
[7]A. Hickman, R. Chaudhuri, S. J. Bader, K. Nomoto, K. Lee, H. G. Xing, and D. Jena, IEEE Electron Device Lett. **40**, 1293 (2019).
[8]G. Koblmueller, R. Averbeck, L. Geelhaar, H. Riechert, W. Hösler, and P. Pongratz, J. Appl. Phys. **93**, 9591 (2003).
[9]See www.cisuvc.com/products.
[10]Z. Zhang, M. Kushimoto, T. Sakai, N. Sugiyama, L. J. Schowalter, C. Sasaoka, and H. Amano, Appl. Phys. Express **12**, 124003 (2019).
[11]J. Simon, V. Protasenko, C. Lian, H. Xing, and D. Jena, Science **327**, 60 (2010).
[12]A. Rice, R. Collazo, J. Tweedie, R. Dalmau, S. Mita, J. Xie, and Z. Sitar, J. Appl. Phys. **108**, 043510 (2010).
[13]J. H. Dycus, K. J. Mirrielees, E. D. Grimley, R. Kirste, S. Mita, Z. Sitar, R. Collazo, D. L. Irving, and J. M. LeBeau, ACS Appl. Mater. Interfaces **10**, 10607 (2018).
[14]G. Renaud, B. Villette, I. Vilfan, and A. Bourret, Phys. Rev. Lett. **73**, 1825 (1994).
[15]C. Barth and M. Reichling, Nature **414**, 54 (2001).
[16]R. Page, J. Casamento, Y.-J. Cho, S. Rouvimov, H. G. Xing, and D. Jena, Phys. Rev. Mater. **3**, 064001 (2019).
[17]Y.-J. Cho, A. Summerfield, A. Davies, T. S. Cheng, E. F. Smith, C. J. Mellor, A. N. Khlobystov, C. T. Foxon, L. Eaves, P. H. Beton, and S. Novikov, Sci. Rep. **6**, 34474 (2016).
[18]Y. Asaoka, J. Cryst. Growth **251**, 40 (2003).
[19]Z. Wasilewski, J.-M. Baribeau, M. Beaulieu, X. Wu, and G. Sproule, J. Vac. Sci. Technol., B **22**, 1534 (2004).
[20]L. Li, E. Linfield, R. Sharma, and A. Davies, Appl. Phys. Lett. **99**, 061910 (2011).
[21]T. Xia, Y.-J. Cho, M. Cotrufo, I. Agafonov, F. Van Otten, and A. Fiore, Semicond. Sci. Technol. **30**, 055009 (2015).
[22]V. Laurent, D. Chatain, C. Chatillon, and N. Eustathopoulos, Acta Metall. **36**, 1797 (1988).
[23]N. Eustathopoulos, M. G. Nicholas, and B. Drevet, *Wettability at High Temperatures* (Elsevier, 1999), Vol. 3.
[24]S. G. Mueller, R. T. Bondokov, K. E. Morgan, G. A. Slack, S. B. Schujman, J. Grandusky, J. A. Smart, and L. J. Schowalter, Phys. Status Solidi A **206**, 1153 (2009).
[25]L. I. Berger, *Semiconductor Materials* (CRC Press, 1996), p. 123.
[26]A. Y. Cho, J. Cryst. Growth **201–202**, 1 (1999).
[27]T. Van Buuren, M. Weilmeier, I. Athwal, K. Colbow, J. Mackenzie, T. Tiedje, P. Wong, and K. Mitchell, Appl. Phys. Lett. **59**, 464 (1991).
[28]C. Adelmann, J. Brault, D. Jalabert, P. Gentile, H. Mariette, G. Mula, and B. Daudin, J. Appl. Phys. **91**, 9638 (2002).
[29]C. Adelmann, J. Brault, G. Mula, B. Daudin, L. Lymperakis, and J. Neugebauer, Phys. Rev. B **67**, 165419 (2003).
[30]O. Brandt, Y. J. Sun, L. Däweritz, and K. H. Ploog, Phys. Rev. B **69**, 165326 (2004).
[31]C. Lee, Y. Dong, R. M. Feenstra, J. E. Northrup, and J. Neugebauer, Phys. Rev. B **68**, 205317 (2003).
[32]M. D. Brubaker, S. M. Duff, T. E. Harvey, P. T. Blanchard, A. Roshko, A. W. Sanders, N. A. Sanford, and K. A. Bertness, Cryst. Growth Des. **16**, 596 (2016).
[33]A. Smith, d. R. Feenstra, D. Greve, M.-S. Shin, M. Skowronski, J. Neugebauer, and J. Northrup, Appl. Phys. Lett. **72**, 2114 (1998).
[34]A. Meldrum, S. Honda, C. White, R. Zuhr, and L. Boatner, J. Mater. Res. **16**, 2670 (2001).
[35]J. Ben, X. Sun, Y. Jia, K. Jiang, Z. Shi, H. Liu, Y. Wang, C. Kai, Y. Wu, and D. Li, CrystEngComm **20**, 4623 (2018).
[36]P. Mazzolini, P. Vogt, R. Schewski, C. Wouters, M. Albrecht, and O. Bierwagen, APL Mater **7**, 022511 (2019).
[37]M. Binnewies and E. Milke, *Thermochemical Data of Elements and Compounds* (Wiley-VCH, 1999).

**SUPPLEMENTARY INFORMATION for**

# Molecular beam homoepitaxy on bulk AlN enabled by aluminum-assisted surface cleaning

YongJin Cho,[1,a)] Celesta S. Chang,[2,3] Kevin Lee,[1] Mingli Gong,[4] Kazuki Nomoto,[1] Masato Toita,[5] Leo J. Schowalter,[5] David A. Muller,[3,6] Debdeep Jena,[1,4,6] and Huili Grace Xing [1,4,6]

[1]*School of Electrical and Computer Engineering, Cornell University, Ithaca, New York 14853, USA*
[2]*Department of Physics, Cornell University, Ithaca, New York 14853, USA*
[3]*School of Applied and Engineering Physics, Cornell University, Ithaca, New York 14853, USA*
[4]*Department of Materials Science and Engineering, Cornell University, Ithaca, New York 14853, USA*
[5]*Crystal IS, Green Island, New York 12183, USA*
[6]*Kavli Institute for Nanoscale Science, Cornell University, Ithaca, New York 14853, USA*

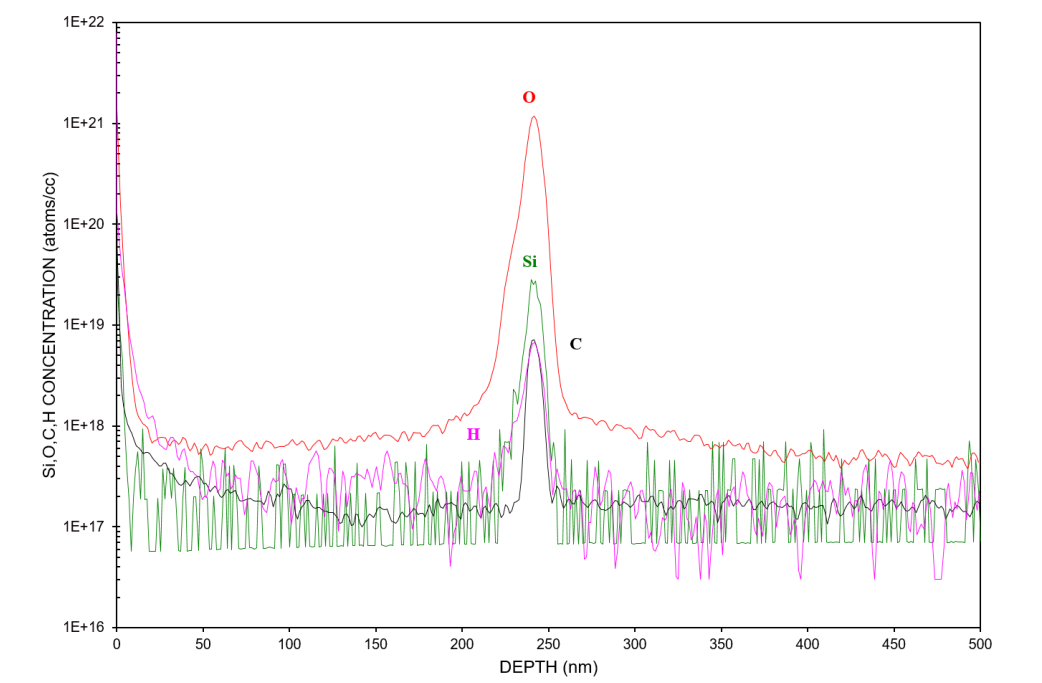


Fig. S1 SIMS data of the control sample that is AlN grown on AlN wafer without in-situ cleaning.

[a)] Electronic mail: yongjin.cho@cornell.edu

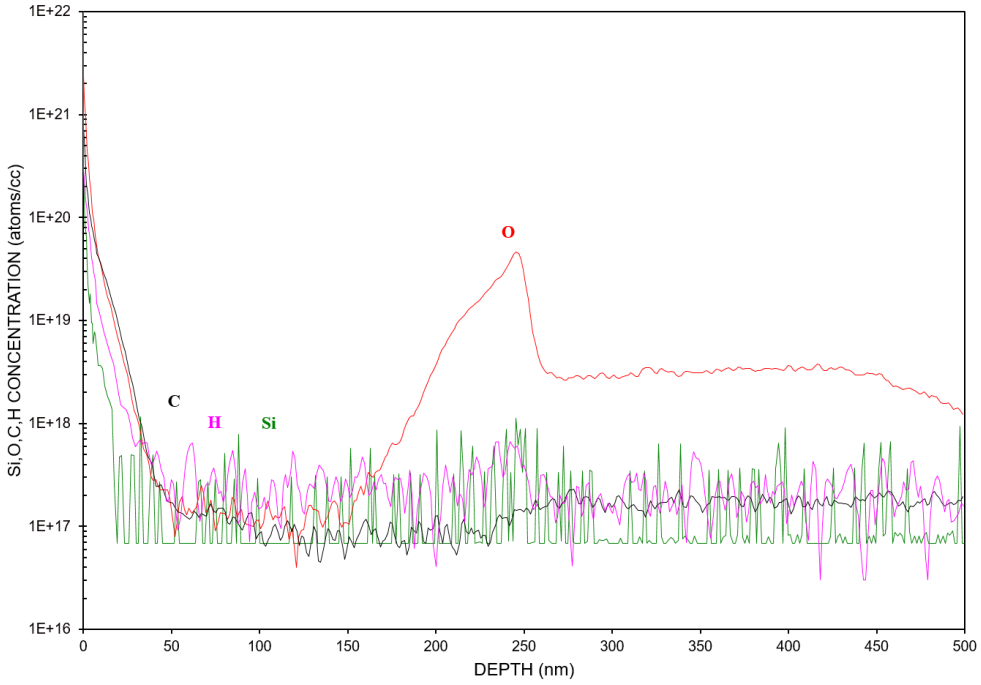


Fig. S2 SIMS data of the thermally cleaned sample.

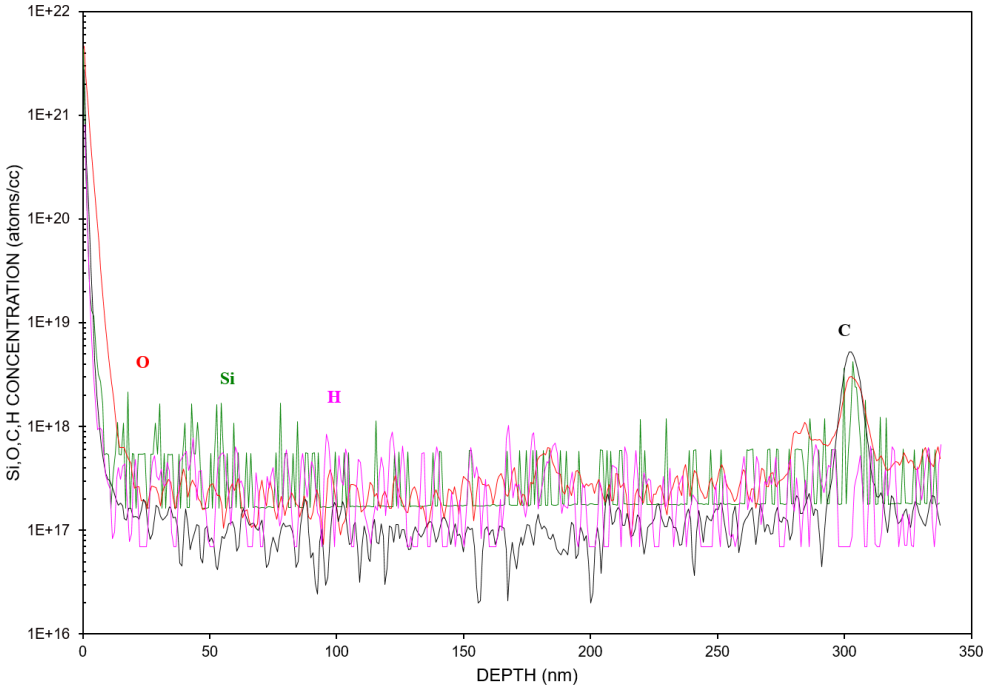


Fig. S3 SIMS data of the Al-assisted cleaned sample.

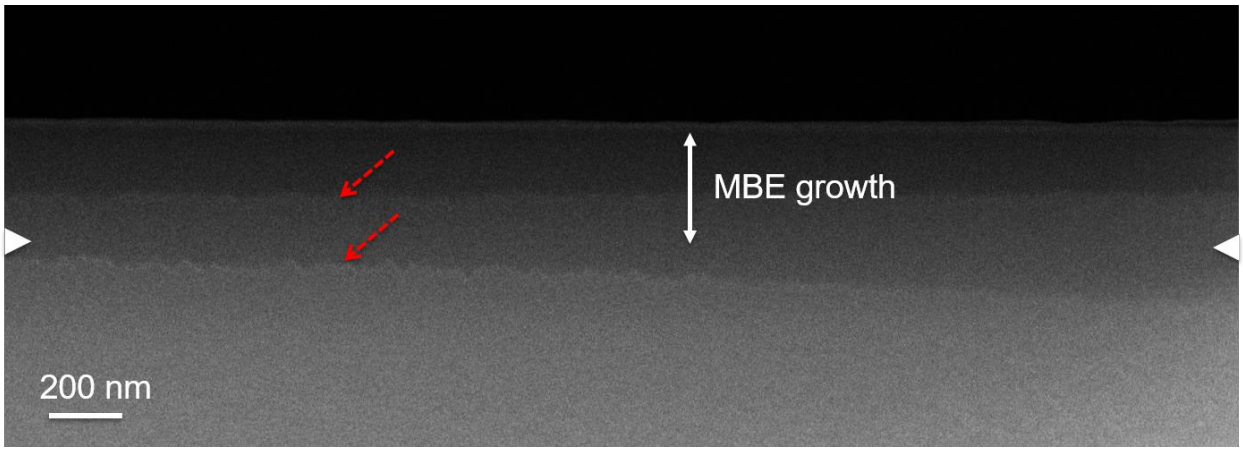


Fig. S4 Low magnification TEM micrograph of the Al-assisted cleaned sample. The red dashed arrows indicate two layers formed by milling with focused ion beam. The notches on the sides indicates the AlN epilayer/wafer interface.